USGS
science for a changing world

AT-SATELLITE REFLECTANCE: A FIRST ORDER NORMALIZATION OF LANDSAT 7 ETM+ IMAGES

Chengquan Huang*, Limin Yang, Collin Homer, Bruce Wylie, James Vogelman
and Thomas DeFelice

Raytheon ITSS, EROS Data Center
Sioux Falls, SD 57198, USA
*Email: huang@edcmail.cr.usgs.gov

U.S. Department of the Interior
U.S. Geological Survey

Abstract: Regional Landsat applications often rely on clear and near cloud-free images. With the spectral value being represented by digital number (DN), however, such images contain substantial noises. A significant proportion of such noises can be normalized by converting the DN to at-satellite reflectance value. Being physically based and ready to automate, the conversion method can serve as a first order normalization of Landsat 7 images, making it possible to derive land surface information from such images more consistently.

Key word: Landsat 7, ETM+, image normalization, digital number, at-satellite reflectance.

1. Introduction

One of the challenges to satellite-based land cover characterization is removing or normalizing the noises arising from atmospheric effect, changing view and illumination geometry, and instrument errors (Wharton 1989). Such noises hinder the ability to derive land surface information reliably and consistently. Great efforts have been made to minimize instrument errors for standard image products of Landsat 7 Enhanced Thematic Mapper Plus (ETM+) (Irish 2000). Noises due to the impact of the atmospheric and illumination geometry can be normalized in several approaches. One is atmospheric correction (e.g. Moran et al. 1992, Liang et al. 1997), the applicability of which to large area applications is limited due to lack of in-situ measurements of atmospheric conditions for many applications and uncertainties associated with current atmospheric correction algorithms. Another approach relies on pseudo-invariant objects (Schott et al. 1988, Heo and FitzHugh 2000). This approach assumes that the spectral properties of pseudo-invariant objects do not change significantly over time. Their spectral values are used to normalize scenes to a base image using regression techniques. A problem with this approach is the difficulty to automate because pseudo-invariant objects have to be identified manually. Besides, results of this approach can be biased when the selected pseudo-invariant objects are not rigorously invariant.

In this study, we demonstrate that for clear and near cloud-free ETM+ images, a first order normalization can be achieved by converting the raw digital number (DN) to at-satellite reflectance. The conversion algorithm is physically based, ready to automate, and does not introduce errors to the data.

2. Data and methods

2.1 Image data

A set of 10 ETM+ near cloud-free scenes representing a range of landscapes of the mid-latitude United States were used to test the robustness of the conversion method for image normalization (table 1). Five of the images were acquired during summer and five during fall or winter, representing leaf-on and leaf-off conditions, respectively. These images were radiometrically and geometrically corrected in the EROS Data Center of the U.S. Geological Survey (USGS) using standard methods (Irish 2000).

2.2 Converting DN to at-satellite reflectance

Without considering the impact of topography (Ekstrand 1996) and the atmosphere (Liang et al. 1997), Markham and Barker (1986) gave the two equations for converting DN to at-satellite reflectance:

$$L_\lambda = Gain_\lambda \cdot DN_\lambda + Bias_\lambda \quad (1)$$

$$\rho_\lambda = \frac{\pi \cdot L_\lambda \cdot d^2}{ESUN_\lambda \cdot \sin(\theta)} \quad (2)$$

where L and ρ are at-satellite radiance and reflectance respectively. The subscript λ refers to spectral band λ. For each Landsat7 ETM+ image the gains, biases and sun elevation (θ) are provided in the header file that accompanies the image. The Solar irradiance $ESUN_\lambda$ is given in the Landsat 7 Science Data Users Handbook (Irish 2000). The normalized Sun-Earth distance d for any day of the year can be calculated from the eccentricity correction factor E_0:

$$d^2 = 1/E_0 \quad (3)$$

E_0 can be found from table 1.2.1 or calculated according to equations (1.2.1) and (1.2.2) of Iqbal (1983).

2.3 Noise quantification

The absolute value of the noise in an image is difficult to quantify because simultaneous ground measurements are often unavailable. Relevant to many regional Landsat applications is the relative magnitude of the noise, referred to as relative noise hereafter, among the scenes used. For a pair of images of the same location, one acquired during leaf-on season and the other during leaf-off season, the relative noise between them can be measured using pseudo-invariant objects whose reflective properties are relatively stable over time:

(4)

$$NOISE = \frac{\sqrt{\frac{1}{N}\sum (d1_i - d2_i)^2}}{\max(d1_i, d2_i) - \min(d1_i, d2_i)} \times 100\%$$

where N is the number of pseudo-invariant pixels identified in the image pair, and $d1$ and $d2$ their spectral values (DN or at-satellite reflectance) in the leaf-on and leaf-off images respectively. The relative noises between the pair of DN images ($NOISE_{DN}$) and at-satellite reflectance images ($NOISE_{ref}$) should be roughly comparable, because the magnitude of the noise measured by the numerator of equation (4) is normalized by the range of the spectral value of the pseudo-invariant objects.

Examples of pseudo-invariant objects used in this study include large flat building roofs, airport runways, deep water and stable sand hills. Depending on availability, up to more than one hundred pseudo-invariant objects were manually identified from each of the 5 ETM+ image pairs. Where necessary, 1 meter digital orthophoto quadrangles (DOQ) developed by the USGS were used to aid the selection of those objects.

3. Results and discussion

Figure 1 compares the spectral value of pseudo-invariant objects as measured by the Landsat 7 ETM+ sensor during leaf-on and leaf-off seasons. These objects were selected from the northern Nebraska image pair (path 31/row 30). Due to length limitation, figures generated using the pseudo-invariant objects from the other four image pairs are not presented. They were generally similar to figure 1, though the magnitude of the difference between leaf-on and leaf-off values varied. In general, the pseudo-invariant objects were not temporally invariant when measured by DN (figure 1(a)). The bright objects had substantially higher DN values during the leaf-on season than during the leaf-off season. While some of the pseudo-invariant objects might not be rigorously invariant over time, the majority

of the temporal variations of their DN value should not arise from ground targets, but from changes in other factors including atmospheric effect and illumination angle (table 1). The variations were substantially reduced after the DN values were converted to at-satellite reflectance (figure 1(b)). Similar observations were made for the other four image pairs.

Figure 2 gives the *NOISE*s for the six spectral bands of the 5 image pairs. In general, $NOISE_{ref}$ was about 50% or even less of the corresponding $NOISE_{DN}$, suggesting that more than half of the relative noises between clear and cloud-free leaf-on and leaf-off images can be removed by converting DN to at-satellite reflectance. These observations should be valid for previous Landsat systems, provided the appropriate parameters for equations (1) and (2) are available.

Figure 2 suggests that without performing atmospheric correction, substantial relative noises among clear and near cloud-free images can be removed by converting DN to at-satellite reflectance. This can enhance the consistency of land cover characterization in many ways. For regional applications, scene mosaics can be substantially improved by converting DN to at-satellite reflectance (figure 3). At-satellite reflectance images should be more appropriate for land cover and land cover change analysis than DN images (Huang et al. 1998), because the temporal information contained in at-satellite reflectance images is more relevant to the concerned targets than that contained in DN images. At-satellite reflectance also allows the development of a regionally applicable tasseled cap transformation using physically based measurement (Huang et al. 2001).

Further image normalization can be achieved by considering the impact of topographic effect on view and illumination geometry. Due to time limitations we only tried the Lambertian cosine correction method for topographic normalization (Smith et al. 1980), and would not recommend it over areas with high relief because it does not handle extremely low incidence angles adequately. Use of more complex algorithms needs to be further investigated (Ekstrand 1996).

4. Conclusions

Using pseudo-invariant objects, we demonstrated that a significant proportion of the relative noise exists among multi-temporal clear and near cloud-free ETM+ DN images can be removed by converting DN to at-satellite reflectance. Unlike many other normalization algorithms, this method is physically based, ready to automate and does not introduce noise to the normalized images. It can substantially improve the quality of mosaicked imagery, making multi-scene land cover characterization more consistent. These observations should also be valid for previous Landsat systems if appropriate parameters for equations (1) and (2) are available. This method can be further improved by considering the impact of topography on illumination and view geometry.

Acknowledgement: This study is made possible in part by the Raytheon Corporation under U.S. Geological Survey contract 1434-CR-97-CN-40274.

USGS
science for a changing world

Reference

Ekstrand, S., 1996, Landsat TM-based forest damage assessment: correction for topographic effects, *Photogrammetric Engineering & Remote Sensing*, **62**: 151-161.

Heo, J. and FitzHugh, T. W., 2000, A standardized radiometric normalization method for change detection using remotely sensed imagery, *Photogrammetric Engineering & Remote Sensing*, **66**: 173-181.

Huang, C., Townshend, J. R. G., Zhan, X., Hansen, M., DeFries, R., and Solhberg, R., 1998, Developing the spectral trajectories of major land cover change processes, in *Proceedings of SPIE* (Beijing: SPIE), 155-162.

Huang, C., Wylie, B., Homer, C., Yang, L., and Vogelman, J., 2001, A tassled cap transformation for Landsat 7 ETM+ at-satellite reflectance, *International Journal of Remote Sensing*, **Submitted**.

Iqbal, M., 1983, *An introduction to solar radiation* (Toronto: Academic Press).

Irish, R. R., 2000, Landsat 7 science data user's handbook, Report 430-15-01-003-0, National Aeronautics and Space Administration, http://ltpwww.gsfc.nasa.gov/IAS/handbook/handbook_toc.html.

Liang, S., Vallah-Adl, H., Kalluri, S., Jaja, J., Kaufman, Y. J., and Townshend, J. R. G., 1997, An operational atmospheric correction algorithm for Landsat Thematic Mapper imagery over the land, *Journal of Geophysical Research*, **102**: 17173-17186.

Markham, B. L. and Barker, J. L., 1986, Landsat MSS and TM post-calibration dynamic ranges, exoatmospheric reflectances and at-satellite temperatures, *EOSAT Landsat Technical Notes*, **1**: 3-8.

Moran, M. S., Jackson, R. D., Slater, P. N., and Teillet, P. M., 1992, Evaluation of simplified procedures for retrieval of land surface reflectance factors from satellite sensor output, *Remote Sensing of Environment*, **41**: 169-184.

Schott, J. R., Salvaggio, C., and Volghok, W. J., 1988, Radiometric scene normalization using pseudoinvariant features, *Remote Sensing of Environment*, **26**: 1-16.

Smith, J. A., Lin, T. L., and Ranson, K. J., 1980, The Lambertian assumption and Landsat data, *Photogrammetric Engineering & Remote Sensing*, **46**: 1183-1189.

Wharton, S. W., 1989, Knowledge-based spectral classification of remotely sensed image data, In *Theory and applications of optical remote sensing*, edited by G. Asrar (New York: John Wiley & Sons), 548-577.

Table 1 Landsat 7 ETM+ images used in this study

Path	*Row*	*Geographic location*	*Acquisition date*	*Sun elevation θ (°)*
15	34	Virginia, east	Jul. 28, 1999	63
15	34	Virginia, east	Nov. 17, 1999	32
16	34	Virginia, west	Jul. 19, 1999	64
16	34	Virginia, west	Nov. 8, 1999	34
31	30	Northern Nebraska	Jul. 12, 1999	63
31	30	Northern Nebraska	Nov. 17, 1999	26
38	31	Northeastern Utah	Aug. 14, 1999	57
38	31	Northeastern Utah	Oct. 17, 1999	37
46	29	Western Oregon	Aug. 22, 1999	53
46	29	Western Oregon	Dec. 28, 1999	20

Figure captions

Figure 1 A comparison of the spectral value of pseudo-invariant objects identified from the Northern Nebraska scene (path 31/row 30). Each point represents a pseudo-invariant object. The units for both x- and y-axis are DN value for (a) and at-satellite reflectance × 100 (%) for (b).

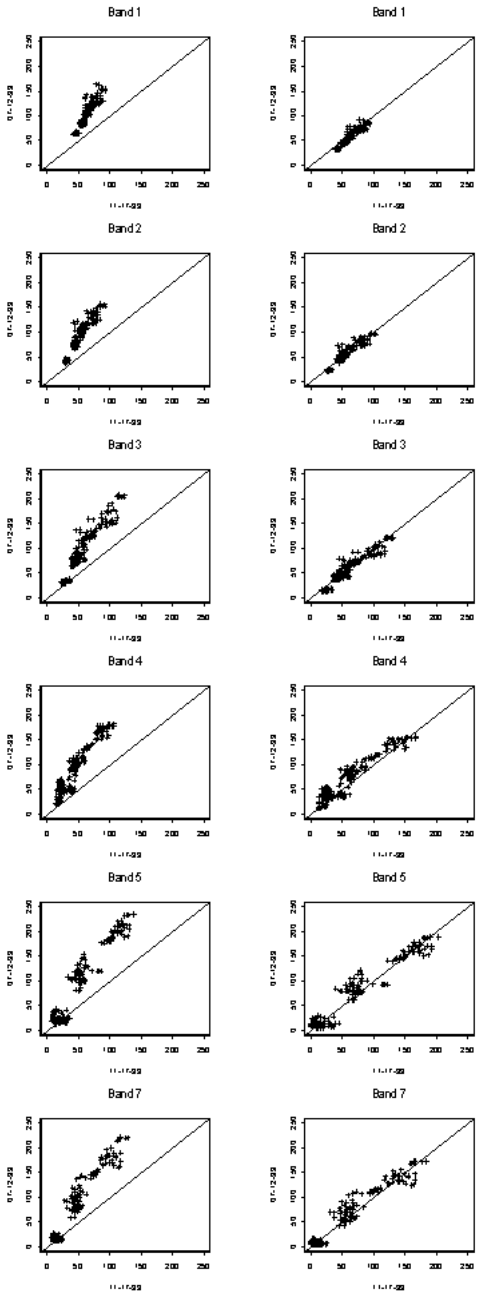

Figure 2 Relative noises between leaf-on and leaf-off images calculated from pseudo-invariant objects using equation (4).

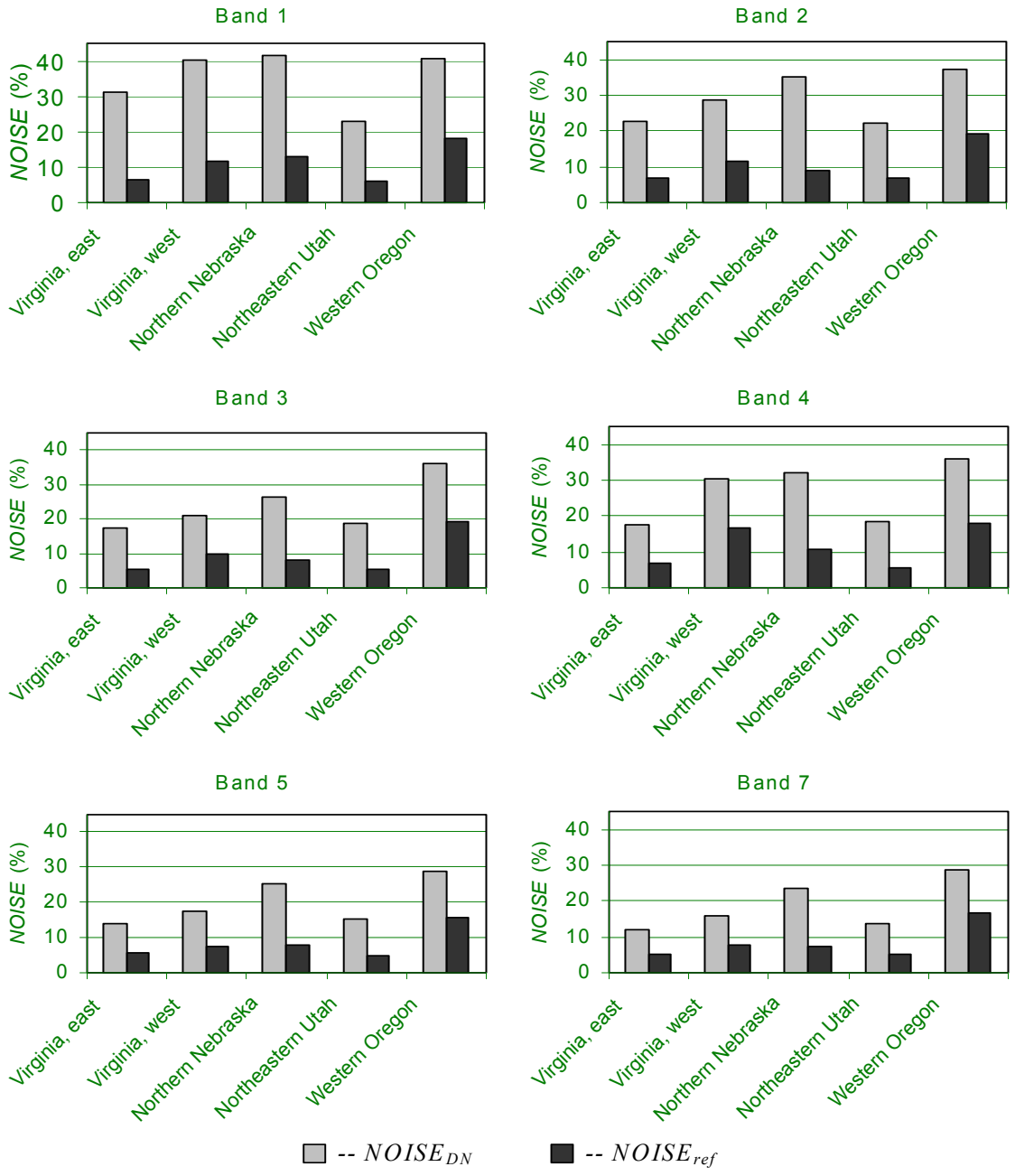

Figure 2

Figure 3 Improvement of at-satellite reflectance over DN in image mosaic. For both (a) and (b) the left mosaics were from DN images and right mosaics from at-satellite reflectance images, and the left scene (path 31/row 30) of each mosaic was acquired on July 12, 1999 and the right scene (path 30/row 30) on August 8, 2000.
(a) In areas where the ground conditions on the scenes to be mosaicked were different, the difference was reduced but did not disappear when DN was converted to at-satellite reflectance.
(b) In areas where the ground conditions on the scenes to be mosaicked were similar, the seam line seen in the DN image mosaic was almost invisible in the at-satellite reflectance image mosaic.

DN image

At-satellite reflectance image

(a)

(b)

Figure 3